



## Original papers

## Proximal hyperspectral sensing and data analysis approaches for field-based plant phenomics

K.R. Thorp<sup>a,\*</sup>, M.A. Gore<sup>b</sup>, P. Andrade-Sanchez<sup>c</sup>, A.E. Carmo-Silva<sup>d</sup>, S.M. Welch<sup>e</sup>, J.W. White<sup>a</sup>, A.N. French<sup>a</sup><sup>a</sup> USDA-ARS, U.S. Arid Land Agricultural Research Center, 21881 N Cardon Ln, Maricopa, AZ 85138, United States<sup>b</sup> Cornell University, Plant Breeding and Genetics Section, School of Integrative Plant Science, 310 Bradfield Hall, Ithaca, NY 14853, United States<sup>c</sup> University of Arizona, Department of Agricultural and Biosystems Engineering, Maricopa Agricultural Center, 37860 W. Smith-Enke Road, Maricopa, AZ 85138, United States<sup>d</sup> Rothamsted Research, Plant Biology and Crop Science Department, Hertsfordshire AL5 2JQ, United Kingdom<sup>e</sup> Kansas State University, Department of Agronomy, 2104 Throckmorton Plant Sciences Center, Manhattan, KS 66506, United States

## ARTICLE INFO

## Article history:

Received 12 February 2015

Received in revised form 18 June 2015

Accepted 6 September 2015

## Keywords:

Cotton

High performance computing

Inverse modeling

Phenotyping

PROSAIL

Remote sensing

## ABSTRACT

Field-based plant phenomics requires robust crop sensing platforms and data analysis tools to successfully identify cultivars that exhibit phenotypes with high agronomic and economic importance. Such efforts will lead to genetic improvements that maintain high crop yield with concomitant tolerance to environmental stresses. The objectives of this study were to investigate proximal hyperspectral sensing with a field spectroradiometer and to compare data analysis approaches for estimating four cotton phenotypes: leaf water content ( $C_w$ ), specific leaf mass ( $C_m$ ), leaf chlorophyll  $a + b$  content ( $C_{ab}$ ), and leaf area index (LAI). Field studies tested 25 Pima cotton cultivars grown under well-watered and water-limited conditions in central Arizona from 2010 to 2012. Several vegetation indices, including the normalized difference vegetation index (NDVI), the normalized difference water index (NDWI), and the physiological (or photochemical) reflectance index (PRI) were compared with partial least squares regression (PLSR) approaches to estimate the four phenotypes. Additionally, inversion of the PROSAIL plant canopy reflectance model was investigated to estimate phenotypes based on 3.68 billion PROSAIL simulations on a supercomputer. Phenotypic estimates from each approach were compared with field measurements, and hierarchical linear mixed modeling was used to identify differences in the estimates among the cultivars and water levels. The PLSR approach performed best and estimated  $C_w$ ,  $C_m$ ,  $C_{ab}$ , and LAI with root mean squared errors (RMSEs) between measured and modeled values of 6.8%, 10.9%, 13.1%, and 18.5%, respectively. Using linear regression with the vegetation indices, no index estimated  $C_w$ ,  $C_m$ ,  $C_{ab}$ , and LAI with RMSEs better than 9.6%, 16.9%, 14.2%, and 28.8%, respectively. PROSAIL model inversion could estimate  $C_{ab}$  and LAI with RMSEs of about 16% and 29%, depending on the objective function. However, the RMSEs for  $C_w$  and  $C_m$  from PROSAIL model inversion were greater than 30%. Compared to PLSR, advantages to the physically-based PROSAIL model include its ability to simulate the canopy's bidirectional reflectance distribution function (BRDF) and to estimate phenotypes from canopy spectral reflectance without a training data set. All proximal hyperspectral approaches were able to identify differences in phenotypic estimates among the cultivars and irrigation regimes tested during the field studies. Improvements to these proximal hyperspectral sensing approaches could be realized with a high-throughput phenotyping platform able to rapidly collect canopy spectral reflectance data from multiple view angles.

Published by Elsevier B.V.

## 1. Introduction

To improve food security, adapt to climate change, and reduce resource requirements for crop production, scientists must better understand the connection between a plant's observable characteristics (phenotype) and its genetic makeup (genotype). Unprece-

dent advances in DNA sequencing have unlocked the genetic code for many important food crops, including rice (*Oryza sativa* L.), sorghum (*Sorghum bicolor* L.), and maize (*Zea mays* L.) (Bolger et al., 2014). However, understanding how genes control complex plant traits, such as drought tolerance, time to anthesis, and harvestable yield, remains challenging. Field-based plant phenomics seeks to implement information technologies, including sensing and computing tools in combination with genetic mapping approaches, to rapidly characterize the physiological responses of

\* Corresponding author.

E-mail address: [kelly.thorp@ars.usda.gov](mailto:kelly.thorp@ars.usda.gov) (K.R. Thorp).

genetically diverse plant populations in the field and relate these responses to individual genes (Araus and Cairns, 2014; Furbank and Tester, 2011; Houle et al., 2010; Montes et al., 2007; White et al., 2012). When validated, crop improvement strategies based on targeted quantitative trait loci and genomic selection can be used for efficient development of crop cultivars that are both high yielding and resilient to environmental stresses.

A variety of electronic sensors have been deployed for field-based plant phenomics, mainly on ground-based vehicles. Andrade-Sanchez et al. (2014) developed a sensing platform on a high-clearance tractor that collected data over four Pima cotton (*Gossypium barbadense* L.) rows simultaneously. Ultrasonic sensors, infrared radiometers, and active multispectral radiometers were used to measure canopy height, temperature, and reflectance, respectively. Scotford and Miller (2004) mounted passive two-band radiometers and ultrasonic sensors on a tractor boom and used the system to estimate tiller density and leaf area index (LAI) of winter wheat (*Triticum aestivum* L.). Other sensing systems have incorporated passive hyperspectral radiometers (spectroradiometers) for measuring crop canopy spectral reflectance continuously over a range of wavelengths, typically within the visible and near-infrared spectrum. For example, the phenotyping platform of Comar et al. (2012) incorporated four spectroradiometers sensitive between 400 and 1000 nm at 3 nm spectral resolution and two RGB digital cameras. Also, Montes et al. (2011) developed a system with light curtains for canopy profiling and spectroradiometers sensitive between 320 and 1140 nm at 10 nm spectral resolution. Rundquist et al. (2004) compared machine-based versus hand-held deployment of a spectroradiometer and found reduced variability and higher reproducibility of sensor measurements when the instrument was positioned by a machine.

Following sensor platforms, the next challenge for field-based plant phenomics is the development of methodologies to extract meaningful information from the sensor data, with the ultimate goal to quantify specific crop phenotypes. However, the fundamental measurements of many sensors have little utility for crop phenotyping without additional post-processing and analysis. For simple, empirical processing of canopy spectral reflectance data, a multitude of vegetation indices have been developed (Bannari et al., 1995) and used to estimate several crop characteristics, including canopy cover, LAI, and biomass (Wanjura and Hatfield, 1987). The popular normalized difference vegetation index (NDVI) is traditionally calculated as

$$\text{NDVI} = \frac{\rho_2 - \rho_1}{\rho_2 + \rho_1} \quad (1)$$

where  $\rho_2$  is the spectral reflectance in the near-infrared waveband and  $\rho_1$  is the spectral reflectance in the red waveband. However, with the advent of hyperspectral sensors, other narrow-band indices have been developed using the NDVI equation with reflectance data in different wavebands. For example, Gamon et al. (1992) developed the physiological (or photochemical) reflectance index (PRI), a narrow-band index using reflectance at 531 nm to track xanthophyll cycle pigments and estimate photosynthetic efficiency. Likewise, Gao (1996) developed the normalized difference water index (NDWI) to estimate vegetation water content. Many other studies have identified optimum wavebands for a given application by calculating narrow-band NDVI for all possible waveband combinations for a given hyperspectral sensor (Fu et al., 2014; Hansen and Schjoerring, 2003; Thenkabail et al., 2000; Thorp et al., 2004). Babar et al. (2006) demonstrated several narrow-band spectral reflectance indices that explained genetic variability in wheat biomass. Mistele and Schmidhalter (2008) measured spectral reflectance of maize canopies from four view angles and found

the spectral reflectance indices were strongly correlated ( $0.57 \leq r^2 \leq 0.91$ ) with total nitrogen uptake and dry biomass weight. In a study by Gutierrez et al. (2012), spectral reflectance indices explained over 87% and 93% of the variability in biomass and LAI, respectively, for three upland cotton varieties. Seelig et al. (2008) correlated shortwave infrared spectral reflectance indices with relative water content and thickness of peace lily (*Spathiphyllum lynnise*) leaves ( $r^2 > 0.94$ ).

Other spectral data analysis approaches consider all the visible, near-infrared, and shortwave infrared wavebands collectively. Statistical procedures such as principal component regression (PCR) and partial least squares regression (PLSR) reduce dimensionality by decomposing the hyperspectral data into a set of independent factors, against which crop biophysical traits are regressed. For example, Thorp et al. (2008) used PCR to estimate maize stand density from aerial hyperspectral imagery ( $r^2 = 0.79$ ). Also, Thorp et al. (2011) used proximal spectral reflectance data with PLSR to estimate dry biomass weight, flower counts, and silique counts of *Lesquerella* (*Lesquerella fendleri*) with root mean squared errors of prediction equal to 2.1 Mg ha<sup>-1</sup>, 251 flowers, and 1018 siliques, respectively. In another study, PLSR models developed from spectral reflectance of rice canopies explained up to 71% of the variability in plant nitrogen (Bajwa, 2006). Hansen and Schjoerring (2003) compared estimates of wheat biophysical variables using (1) linear regression on narrow-band NDVI with optimal wavebands and (2) PLSR with all wavebands from 400 to 900 nm. The NDVI approach better estimated LAI and chlorophyll concentration, while the PLSR approach better estimated green biomass weight and nitrogen concentration.

Another potential solution for quantifying crop phenotypes involves combining measured spectral reflectance data with physical models of radiative transfer in the plant canopy. Input parameters for such models describe attributes (i.e., phenotypes) of the crop canopy, which are used to simulate canopy spectral reflectance. For example, with 14 input parameters that describe plant characteristics and illumination conditions, the PROSAIL model (Jacquemoud et al., 2009) can simulate plant canopy spectral reflectance from 400 to 2500 nm in 1 nm wavebands. Using model inversion techniques, spectral reflectance measurements from spectroradiometers can be used to estimate PROSAIL input parameters. These estimates represent additional crop phenotypes that could be useful in subsequent genetic analyses. By linking crop phenotypes to sensor data through the theoretical knowledge contained in the simulation model, the approach is less empirical than the vegetation index and PLSR approaches.

Literature provides examples of PROSAIL model inversion for vegetation characterization in diverse environments, but field-based plant phenomics is a novel application. Jacquemoud (1993) first investigated the practical limitations of PROSAIL model inversion using synthetic spectra. A subsequent study tested field spectroradiometer data with PROSAIL model inversion to retrieve sugar beet (*Beta vulgaris*) canopy characteristics, such as chlorophyll *a + b* concentration, leaf water thickness, LAI, and leaf inclination angle (Jacquemoud et al., 1995). At coarser spatial and spectral scales, Zarco-Tejada et al. (2003) used data from the Moderate Resolution Imaging Spectroradiometer (MODIS) satellite to invert PROSAIL for estimation of chaparral vegetation water content in a central California shrub land. Yang and Ling (2004) estimated leaf water thickness of New Guinea impatiens (*Impatiens hawkeri*) in a controlled environment using PROSAIL model inversion from 1300 nm to 2500 nm, but spectral artifacts between 400 and 1300 nm due to artificial lighting prevented the estimation of other plant characteristics. PROSAIL model inversion also provided estimates of LAI and chlorophyll *a + b* concentration for potato (*Solanum tuberosum* L.) and wheat managed with variable nitrogen fertilization rates (Botha et al., 2007, 2010). Others have linked

PROSAIL with dynamic models of crop growth and development for wheat (Thorp et al., 2012) and maize (Koetz et al., 2005), which permitted model inversion using time-series spectral reflectance measurements of the crop canopy.

In many previous studies, iterative optimization was used to solve the PROSAIL model inversion problem (Botha et al., 2007, 2010; Jacquemoud et al., 1995; Thorp et al., 2012; Yang and Ling, 2004; Zarco-Tejada et al., 2003). Optimization aims to find solutions in a computationally efficient manner, but convergence to local minimums is a risk. Others have used lookup tables to solve the inversion problem (Combal et al., 2003; Darvishzadeh et al., 2012; Koetz et al., 2005). Lookup tables are a relatively simple way to characterize model responses, but the computational expense can be great if many simulations are required to adequately characterize the parameter space. High-performance computers increase the practicality of the lookup table approach.

The goal of this study was to assess the utility of proximal hyperspectral data and related data analysis techniques for estimating crop phenotypes among Pima cotton cultivars grown in Arizona field studies. Specific objectives were (1) to compare NDVI, NDWI, PRI, PLSR, and PROSAIL model inversion methods to estimate leaf water thickness, specific leaf mass, chlorophyll  $a + b$  concentration, and LAI in cotton and (2) to assess differences between phenotypic estimates among irrigation and cultivar treatments imposed during the field studies.

## 2. Materials and methods

### 2.1. Field experiments

As described in detail by Andrade-Sanchez et al. (2014), field experiments were conducted during the summers of 2010, 2011, and 2012 at the Maricopa Agricultural Center (33.068°N, 111.971°W, 360 m above mean sea level) near Maricopa, Arizona. Twenty-five Pima cotton cultivars were grown under well-watered (WW) and water-limited (WL) conditions using a  $5 \times 5$  lattice design with four replications per treatment. Experimental units were one row with length of 8.8 m and row spacing of 1.02 m. A subset of four cotton cultivars in 2010 (Monseratt Sea Island, Pima 32, Pima S-6, and Pima S-7) and five cotton cultivars in 2011 and 2012 (89590, Monseratt Sea Island, P62, PSI425, and Pima S-6) were selected for intensive field measurements and proximal hyperspectral data collection. These cultivars were chosen based on their different release dates to increase the range of expected responses to heat and water deficit (Carmo-Silva et al., 2012). Subsurface drip irrigation methods were used with irrigation schedules determined from a daily soil water balance model based on FAO-56 methods (Allen et al., 1998). When 50% of treatment plots had one visible flower, the WL treatment received one-half the irrigation rate of the WW treatment.

### 2.2. Field data collection

Intensive field data collection to characterize leaf water content and canopy spectral reflectance for the selected Pima cultivars occurred on five occasions during the three field experiments (Table 1). Measurements were collected in August during the cotton boll filling period. Collection times in 2011 and 2012 were focused in the morning hours after the 2010 data analysis revealed larger differences in relative leaf water content between WW and WL treatments earlier in the day (Carmo-Silva et al., 2012).

During each data collection outing, ground-based radiometric measurements were collected over the selected Pima cultivars using a hand-held field spectroradiometer (Fieldspec 3, Analytical Spectral Devices, Inc., Boulder, CO, USA). Radiometric information was reported in 2151 narrow wavebands from 350 to 2500 nm in 1 nm intervals. The instrument was equipped with a 25° field-of-view fiber optic. To avoid soil background effects, a wand constructed from PVC tubing was used to position the fiber optic at a nadir view angle approximately 0.25 m above the canopy. Because of the proximity of the sensor to the target, the methods are termed “proximal sensing” as opposed to “remote sensing.” Frequent radiometric observations of a calibrated, 0.6 m<sup>2</sup>, 99% Spectralon panel (Labsphere, Inc., North Sutton, New Hampshire) were used to characterize incoming solar radiation throughout the data collection period. Because atmospheric absorption led to insufficient light in some wavebands, subsequent analyses of all spectral data used 1703 wavebands from 400 to 1350 nm, 1450 to 1770 nm, and 1970 to 2400 nm. Canopy reflectance factors in each waveband were computed as the ratio of the canopy radiance over the corresponding time-interpolated value for Spectralon panel radiance. Reflectance factors from six to twelve radiometric measurements over each experimental plot were averaged to estimate the overall canopy spectral reflectance response. Variability in the number of scans per plot was dependent on manual triggering of the spectroradiometer while slowly walking through the field.

Simultaneously with canopy spectral reflectance measurements, two leaf tissue samples were collected from two leaves in each plot with a 2 cm<sup>2</sup> punch. Two leaf disks were collected per sample from one leaf at the top of the canopy, sealed in a  $3 \times 4$  cm<sup>2</sup> pre-weighed ziplock bag, and stored on ice in an insulated cooler. In the laboratory, the fresh weight of leaf samples ( $m_f$ ) was measured on an electronic balance (AE 160, Mettler-Toledo, LLC, Columbus, OH, USA). Leaf disks were then removed from the bags and oven dried prior to dry weight ( $m_d$ ) measurements. The leaf water thickness ( $C_w$ ) was calculated as the depth of water per unit leaf area (cm):

$$C_w = (m_f - m_d) / (\rho_w \times A_{ls}) \quad (2)$$

**Table 1**

Field measurement schedule for five cotton phenomics data sets: 2010A, 2010B, 2011, 2012A, and 2012B.<sup>a</sup>

Measurement	2010A	2010B	2011	2012A	2012B
Leaf punches for $C_w$ and $C_m$	04 August 2010 09:00–10:30	04 August 2010 13:30–16:30	18 August 2011 09:00–10:30	03 August 2012 08:45–10:30	31 August 2012 09:00–11:00
Leaf punches for $C_{ab}$	30 July 2010 morning	30 July 2010 morning	10 August 2011 morning	09 August 2012 08:30–10:45	16 August 2012 7:45–11:00
Fieldspec canopy spectral reflectance	04 August 2010 08:00–09:45	04 August 2010 14:00–15:30	18 August 2011 09:00–10:30	03 August 2012 08:45–10:30	31 August 2012 09:00–11:00
Crop Circle canopy reflectance	05 August 2010 14:00–15:15	05 August 2010 14:00–15:15	18 August 2011 15:00–15:45	02 August 2012 07:00–08:30	31 August 2012 10:00–11:30
Manual canopy height	08 August 2010 morning	08 August 2010 morning	19 August 2011 morning	02 August 2012 morning	30 August 2012 morning

<sup>a</sup> Leaf chlorophyll  $a + b$  content,  $C_{ab}$ ; leaf water thickness,  $C_w$ ; specific leaf mass,  $C_m$ .

where  $\rho_w$  is the density of water ( $1.0 \text{ g cm}^{-3}$ ) and  $A_{ls}$  is the total area of the leaf sample. The specific leaf mass ( $C_m$ ,  $\text{g cm}^{-2}$ ) was also calculated:

$$C_m = m_d/A_{ls} \quad (3)$$

Within two weeks of proximal hyperspectral measurements (Table 1), additional leaf samples were collected for measurements of chlorophyll  $a + b$  concentration ( $C_{ab}$ ). Two  $0.3 \text{ cm}^2$  leaf disks were obtained from each experimental plot and stored at  $-80^\circ\text{C}$ . Using the method of Porra et al. (1989), 100% methanol (1 mL) was added to each sample for pigment extraction in the dark at  $4^\circ\text{C}$  for 48 h with mixing. A  $200 \mu\text{L}$  sample of the supernatant was collected for absorbance measurements at  $652 \text{ nm}$  ( $A_{652}$ ) and  $665 \text{ nm}$  ( $A_{665}$ ), which were used to estimate  $C_{ab}$  ( $\mu\text{g cm}^{-2}$ ):

$$C_{ab} = (22.12A_{652} + 2.71A_{665})/A_{ls} \quad (4)$$

Within one day of proximal hyperspectral measurements (Table 1), the field-based high-throughput phenotyping system of Andrade-Sanchez et al. (2014) was used to measure canopy reflectance, height, and temperature in each experimental plot. Sensors were deployed on an open rider sprayer (LeeAgro 3434 DL, LeeAgro, Lubbock, TX, USA) capable of sensing four cotton rows simultaneously. Canopy reflectance was measured in  $10 \text{ nm}$  wavebands centered at  $670$ ,  $720$ , and  $820 \text{ nm}$  using active multispectral radiometers (Crop Circle ACS-470, Holland Scientific, Lincoln, NE, USA). Eq. (1) was used to calculate NDVI from these data with  $\rho_1$  and  $\rho_2$  equal to reflectance values at  $670$  and  $820 \text{ nm}$ , respectively. Although canopy height was measured by the phenotyping platform using sonar proximity sensors (Pulsar dB3, Pulsar Process Measurement Ltd, Malvern, UK), this study used canopy height data measured manually using an electronic bar code scanner with a coded measurement stick. Using the approach of Scotford and Müller (2004), the NDVI from active radiometers and manual canopy height data were used to calculate a compound canopy index (CCI), from which LAI was estimated:

$$\text{LAI} = \beta \times \text{CCI} = \beta \left( \frac{c}{c_{\max}} \right) \left( \frac{h}{h_{\max}} \right) \quad (5)$$

where  $\beta$  is a constant,  $c$  and  $h$  are respectively the instantaneous canopy cover and canopy height measurements, and  $c_{\max}$  and  $h_{\max}$  are respectively the maximum cover and height expected during the growing season. Co-located data to parameterize this calculation were collected during other upland cotton experiments conducted at MAC from 2009 to 2013. Analysis of these data led to values of  $5.5$ ,  $87.9\%$ , and  $110.5 \text{ cm}$  for  $\beta$ ,  $c_{\max}$ , and  $h_{\max}$ , respectively. The NDVI data from the active radiometers were used as a direct estimate of  $c$  in Eq. (5). Compared with 75 measurements from a LAI meter (LAI-2200 Plant Canopy Analyzer, Li-Cor Biosciences, Lincoln, NE, USA) and with LAI calculated using 75 measurements of leaf area from biomass samples on an area meter (LAI-3100, Li-Cor Biosciences, Lincoln, NE, USA), the index estimated LAI with a root mean squared error of  $0.48$  ( $15.9\%$ ).

### 2.3. Vegetation indices

Eq. (1) was used to calculate three vegetation indices from the proximal hyperspectral data. The indices were selected based on their relevance to monitor physiological stress in vegetation. A traditional broad-band NDVI was calculated with  $\rho_1$  and  $\rho_2$  equal to the average spectral reflectance in wavebands corresponding to the red ( $665\text{--}675 \text{ nm}$ ) and NIR ( $815\text{--}825 \text{ nm}$ ) filters used with the Crop Circle reflectance sensors onboard the phenotyping vehicle. The NDWI (Gao, 1996) was calculated with  $\rho_1$  and  $\rho_2$  equal to the average spectral reflectance in wavebands corresponding to MODIS Band 5 ( $1230\text{--}1250 \text{ nm}$ ) and Band 2 ( $841\text{--}876 \text{ nm}$ ), respec-

tively. Finally, the PRI (Gamon et al., 1992) was calculated with  $\rho_1$  and  $\rho_2$  equal to spectral reflectance at  $531 \text{ nm}$  and  $570 \text{ nm}$ , respectively. Linear regression models were developed to estimate  $C_w$ ,  $C_m$ ,  $C_{ab}$ , and LAI using each of these spectral indices. While these three indices were specifically highlighted, Eq. (1) was also used to calculate NDVI for all possible combinations of the 1703 proximal hyperspectral wavebands.

### 2.4. PLSR modeling

PLSR was used to assess the relationships between each of the four biophysical variables and canopy spectral reflectance in 1703 wavebands. Thorp et al. (2011) provided the details on the PLSR methodology used in the present study. Briefly, if  $\mathbf{Y}$  is an  $n \times 1$  vector of responses (measured crop phenotypes) and  $\mathbf{X}$  is an  $n$ -observation by  $p$ -variable matrix of predictors (hyperspectral reflectance measurements in  $p$  wavebands), PLSR aims to decompose  $\mathbf{X}$  into a set of  $A$  orthogonal scores such that the covariance with corresponding  $\mathbf{Y}$  scores is maximized. The  $X$ -weight and  $Y$ -loading vectors that result from the decomposition are used to estimate the vector of regression coefficients,  $\beta_{\text{PLS}}$ , such that

$$\mathbf{Y} = \mathbf{X}\beta_{\text{PLS}} + \epsilon \quad (6)$$

where  $\epsilon$  is an  $n \times 1$  vector of error terms.

The “pls” package (Mevik and Wehrens, 2007) within the R Project for Statistical Computing (<http://www.r-project.org>) was used for PLSR in this study. Four models were developed: one each for estimating  $C_w$ ,  $C_m$ ,  $C_{ab}$ , and LAI from the canopy spectral reflectance data. To choose the appropriate number of factors for each model ( $A$  from above), leave-one-out cross validation was used to test model predictions for independent data, and scree plots (not shown) provided the number of factors for which the root mean squared error of cross validation (RMSECV) was minimized. The PLSR models for  $C_w$ ,  $C_m$ ,  $C_{ab}$ , and LAI were developed from the first five, eight, eight, and ten factors, respectively.

### 2.5. PROSAIL simulations

The PROSAIL canopy reflectance model was developed by linking the PROSPECT leaf optical properties model and the SAIL canopy bidirectional reflectance model (Jacquemoud et al., 2009). PROSAIL uses 14 input parameters to define leaf pigment content, leaf water content, canopy architecture, soil background reflectance, and illumination characteristics. Four of the PROSAIL input parameters are the four biophysical variables measured in this study:  $C_w$ ,  $C_m$ ,  $C_{ab}$ , and LAI. In addition to  $C_{ab}$ , other leaf pigment parameters include the carotenoid content ( $\mu\text{g cm}^{-2}$ ) and the brown pigment content (unitless fraction from  $0.0$  to  $1.0$ ). Another leaf-scale parameter is the leaf structural coefficient ( $N$ ; unitless), defined as the number of leaf mesophyll layers. In addition to LAI, canopy architecture is defined by the average leaf inclination angle ( $\theta_l$ ; degrees). The background soil reflectance parameter ranges from  $0.0$  for wet soils to  $1.0$  for dry soils. Specular properties of the canopy surface are characterized by the hot spot size parameter ( $s$ ; unitless fraction from  $0.0$  to  $1.0$ ). The skylight parameter (%) defines the percentage of diffuse solar radiation. Illumination and viewer geometries are characterized by the solar zenith angle (degrees), viewer zenith angle (degrees), and relative solar and viewer azimuth angle (degrees). Based on these inputs, the model calculates canopy bidirectional reflectance from  $400$  to  $2500 \text{ nm}$  in  $1 \text{ nm}$  increments.

PROSAIL has been developed in several programming languages. Initial simulations were conducted using the Fortran version, which was compiled using the “g95” Fortran compiler (<http://www.g95.org>) on a Linux operating system. Later, PROSAIL for Python was deemed better for the simulation analysis, because

it encapsulated the Fortran code as an extension for the Python programming language (<http://www.python.org>). This permitted the model to be called from the Python command line and eliminated hard disk access requirements for model input and output.

PROSAIL simulations were conducted on the “Stampede” super-computer at the Texas Advanced Computing Center (TACC), located at the University of Texas in Austin. A single job submission was used to conduct 3.68 billion PROSAIL simulations to test the effects of multiple parameter combinations on simulated canopy spectral reflectance. Because proximal hyperspectral measurements were collected in a total of 184 plots over all the field experiments, 184 processing cores were requested such that the simulation analysis could be explicitly conducted for the conditions of each experimental unit. The maximum run time for a job submission on Stampede is 48 h. Thus, the design objective was to conduct as many PROSAIL evaluations as possible within the time limit.

Seven parameters were adjusted during the PROSAIL simulation exercise (Table 2). A Sobol quasirandom sequence algorithm for Python was used to sample the parameter space. Although “less random” than a pseudorandom number sequence, the approach tends to sample the parameter space “more uniformly.” Another advantage is that the sequence is repeatable, so identical parameter combinations could be tested for each experimental unit. For  $C_w$ ,  $C_m$ ,  $C_{ab}$ , and LAI, the lower and upper bounds were specified using the range of measured values. Ranges for  $N$ ,  $\theta_l$ , and  $s$  were specified using published values (Combal et al., 2003; Jacquemoud et al., 1995). Leaf carotenoid content and brown pigment content were less sensitive parameters and were fixed at  $10.0 \mu\text{g cm}^{-2}$  and 0.0 (unitless), respectively. Because subsurface drip irrigation was used, the soil surface was normally dry. Thus, the soil reflectance parameter was fixed at 1.0 for all simulations. The fraction of diffuse skylight was fixed at 10% based on observations of a shaded versus sunlit Spectralon panel during the field study. By implementing the solar position algorithm of Reda and Andreas (2004), solar zenith angles were calculated from the timestamps of radiometric observations in the field. Observer zenith and relative azimuth angles were both fixed at  $0^\circ$ . This approach provided an evaluation of 20 million combinations of seven PROSAIL parameters for each of the 184 experimental units monitored during the field studies.

## 2.6. PROSAIL model inversion

Available storage allocation on Stampede became the limiting factor when PROSAIL simulation results were initially written to the hard drive (i.e., 1703 simulated reflectance values for 3.68 billion simulations would have exceeded the available storage allocation on Stampede). Thus, objective function evaluations were

incorporated into the simulation exercise to reduce storage requirements. Tested parameter sets were stored in a lookup table with their corresponding objective function evaluations, including the root mean squared error (RMSE) and the spectral angle ( $\alpha$ ) (Kruse et al., 1993) between measured and simulated reflectance over all spectral wavebands ( $n = 1703$ ):

$$\text{RMSE} = \sqrt{\sum_{i=1}^n (\mathbf{S}_i - \text{PROSAIL}(\mathbf{P}, \mathbf{C})_i)^2} \quad (7)$$

and

$$\alpha = \cos^{-1} \left( \frac{\sum_{i=1}^n \mathbf{S}_i \times \text{PROSAIL}(\mathbf{P}, \mathbf{C})_i}{\left(\sum_{i=1}^n \mathbf{S}_i^2\right)^{0.5} \left(\sum_{i=1}^n \text{PROSAIL}(\mathbf{P}, \mathbf{C})_i^2\right)^{0.5}} \right) \quad (8)$$

where  $\mathbf{S}$  is the vector of measured canopy spectral reflectance and  $\text{PROSAIL}(\mathbf{P}, \mathbf{C})$  is the vector of simulated canopy spectral reflectance as a function of adjusted parameters,  $\mathbf{P}$ , and constant parameters,  $\mathbf{C}$ . The main advantage of  $\alpha$  is its insensitivity to illumination, because Eq. (8) incorporates only vector direction and not vector length. This was considered advantageous because proximal canopy spectral reflectance measurements were largely affected by the fraction of sunlit versus shaded leaves in the instrument’s field of view. Inversion of the PROSAIL model involved the identification of  $\mathbf{P}$  that minimized each of these objective functions for each experimental unit.

## 2.7. Statistics

For proximal hyperspectral sensing to be useful in field-based plant phenomics, metrics obtained from the data must demonstrate differences among the treatments imposed and be repeatable (i.e., heritable). Different cultivars can then be identified and selected as parents of breeding populations for development of improved cultivars. Hierarchical linear mixed modeling was used to assess differences among all data and metrics evaluated in this study: field measurements, measured spectra, vegetation indices, PLSR results, and estimates from PROSAIL model inversion. Cultivar, water level, and their interaction were modeled as fixed effects. Measurement date (Table 1) and its interaction with both cultivar and water level were modeled as random effects. Replicate plot, nested within measurement date and water level, was also included as a random effect in the model. Hierarchical tests required fitting random effects with (1) cultivar fixed effects alone, (2) water level fixed effects alone, (3) both cultivar and water level fixed effects, and (4) cultivar and water level fixed effects and their interaction. Likelihood ratio tests were used to compare these hierarchical models, which showed whether a given data set was different among cultivars, water levels, or their interaction. Tukey’s multiple comparisons tests were also conducted to identify specific cultivars that were different for a given measurement. Statistics were computed using the “lme4” package within the R Project for Statistical Computing software.

## 3. Results

### 3.1. Field measurements

Measured values for  $C_w$ ,  $C_m$ ,  $C_{ab}$ , and LAI ranged from 0.01 to 0.02 cm, 0.003 to 0.009  $\text{g cm}^{-2}$ , 26.0 to 59.0  $\mu\text{g cm}^{-2}$ , and 1.7 to 8.3, respectively, over all measurements collected (Fig. 1). Hierarchical linear mixed modeling revealed differences in all four measured plant traits among cultivars ( $p < 0.01$ , Table 3). Differences in measured  $C_m$  and LAI were found among the water levels ( $p < 0.05$ ). The interaction of cultivar and water level was significant for  $C_w$  and  $C_m$  ( $p < 0.05$ ). Results for measured  $C_w$  and  $C_m$  corroborate the results of Carmo-Silva et al. (2012), who conducted an

**Table 2**  
Parameterization of the PROSAIL model.

Parameter	Unit	State	Lower bound	Upper bound
Leaf water thickness ( $C_w$ )	cm	Free	0.01	0.02
Specific leaf mass ( $C_m$ )	$\text{g cm}^{-2}$	Free	0.003	0.008
Chlorophyll $a + b$ ( $C_{ab}$ )	$\mu\text{g cm}^{-2}$	Free	25.0	60.0
Leaf area index (LAI)	unitless	Free	1.25	8.75
Leaf structure parameter ( $N$ )	unitless	Free	1.4	2.4
Average leaf angle ( $\theta_l$ )	degrees	Free	10.0	70.0
Hot spot size ( $s$ )	unitless	Free	0.001	1.0
Leaf carotenoid content	$\mu\text{g cm}^{-2}$	Fixed	10.0	10.0
Brown pigment content	unitless	Fixed	0.0	0.0
Soil reflectance parameter	unitless	Fixed	1.0	1.0
Diffuse radiation fraction	%	Fixed	10.0	10.0
Solar zenith angle	degrees	Fixed	27.3	60.3
Viewer zenith angle	degrees	Fixed	0.0	0.0
Relative azimuth angle	degrees	Fixed	0.0	0.0

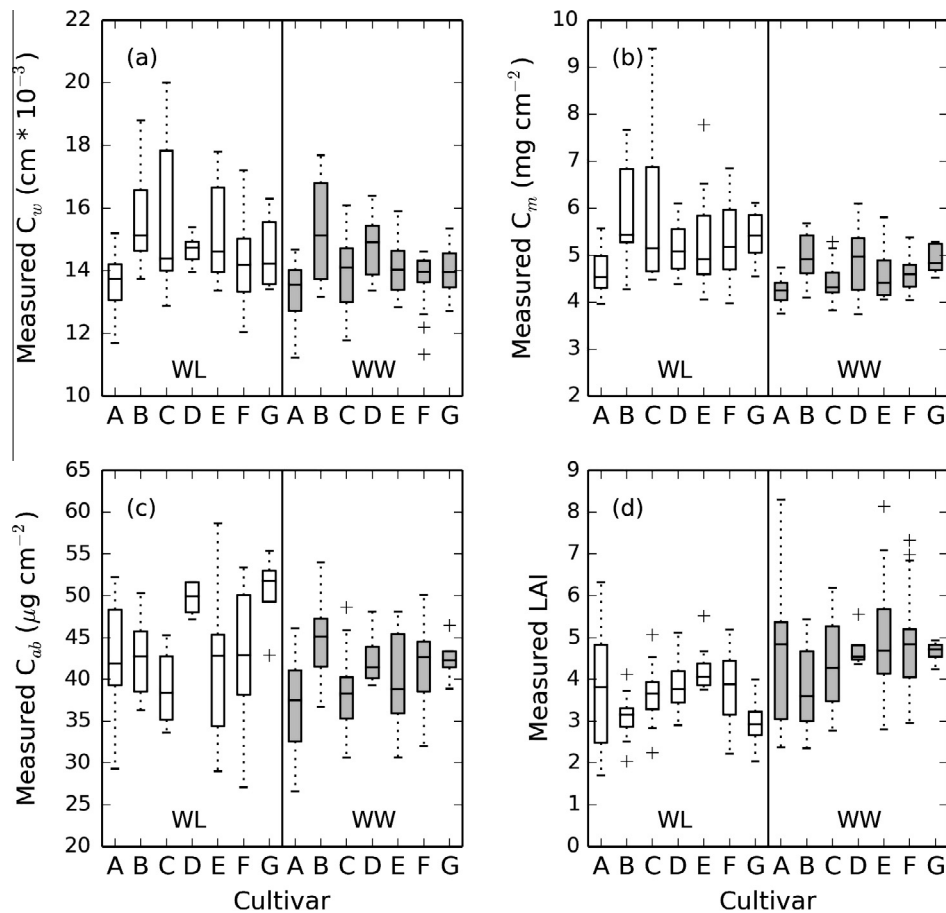


**Fig. 1.** Box plots for (a) leaf water content ( $C_w$ ), (b) specific leaf mass ( $C_m$ ), (c) leaf chlorophyll  $a + b$  content ( $C_{ab}$ ), and (d) leaf area index (LAI) for all measurements collected for the 2010A, 2010B, 2011, 2012A, and 2012B data sets. Measurements were collected under well-watered (WW) and water-limited (WL) conditions for seven Pima cotton cultivars: (A) Monseratt Sea Island, (B) P62, (C) 89590, (D) Pima32, (E) PSI425, (F) Pima S-6, and (G) Pima S-7.

independent analysis using data from the 2010 season only. Typically, the lowest and highest  $C_w$  were found for the Monseratt Sea Island and P62 cultivars, respectively (Fig. 1a), and Tukey tests confirmed  $C_w$  differences between P62 and both Monseratt Sea Island and Pima S-6 for both WW and WL treatments ( $p < 0.05$ ). For WL conditions,  $C_m$  for Monseratt Sea Island was less than four other cultivars: P62, 89590, PSI425, and Pima S-6 ( $p < 0.05$ ). For WW conditions,  $C_m$  was lower for Monseratt Sea Island as compared to P62 ( $p < 0.01$ , Fig. 1b). The  $C_{ab}$  for P62 was greater than both Monseratt Sea Island and 89590 ( $p < 0.05$ ) for WW conditions, but no  $C_{ab}$  differences were found among cultivars for the WL treatment (Fig. 1c). With WW conditions, LAI for P62 was less than that for five other cultivars: Monseratt Sea Island, Pima32, PSI425, Pima S-6, and Pima S-7 ( $p < 0.10$ , Fig. 1d). Also, LAI for 89590 was less than that for Monseratt Sea Island, Pima32, Pima S-6, and Pima S-7 ( $p < 0.05$ ). With WL conditions, LAI for P62 was less than that for Monseratt Sea Island, Pima 32, and Pima S-6. Based on measurements from five data sets, these results highlight the main differences for measured traits among cultivars.

Proximal hyperspectral measurements of the cotton canopy followed typical patterns for spectral reflectance of vegetation (Fig. 2). Generally, scattering of near-infrared radiation led to greater variability in reflectance from 760 to 1350 nm as compared to the visible (400 to 700 nm) and shortwave infrared (1450 to 2400 nm) wavebands where chlorophyll and water, respectively, absorb radiation. Results from hierarchical linear mixed modeling demonstrated the wavebands with different reflectance values among water levels and cultivars ( $p < 0.05$ , Fig. 3). Among culti-

vars, spectral reflectance differences were found in wavebands from 400 to 725 nm, 1470 to 1800 nm, and 2000 to 2400 nm. Thus, reflectance in the entire visible portion of the spectrum was different among cultivars, likely due to effects of radiation absorption by chlorophyll. Also, reflectance differences in two regions of the shortwave infrared suggest effects of  $C_w$  or total plant water status. A fewer number of wavebands demonstrated reflectance differences among water levels, and four main regions were identified: 528–569 nm, 667–736 nm, 1681–1785 nm, and 2153–2353 nm. Wavebands around 550 nm suggested that water level affected greenness of the canopy, while reflectance in the far red and red edge bands were also affected. Reflectance differences in the shortwave infrared bands again suggest effects of water level on plant water status, as expected. Neither cultivar nor water level led to differences in near-infrared reflectance, suggesting that other factors contributed to the variability in those wavebands. There were also no significant cultivar by water level interaction effects on reflectance.

### 3.2. Vegetation indices

Differences in broad-band NDVI from the spectroradiometer were found for both the cultivar and water level treatments (Table 3), demonstrating its robustness for proximal and remote sensing applications in agriculture. Differences in broad-band NDWI were also found among cultivar and water level treatments. Thus, the NDVI and NDWI could collectively provide estimates of both crop growth and water status. No differences in PRI were

**Table 3**

Results of hierarchical linear mixed modeling for measured plant traits, vegetation indices, and plant trait estimates from PLSR models and PROSAIL model inversion.<sup>a</sup>

Trait	Cultivar		Water level		Interaction	
	$\chi^2$	P	$\chi^2$	P	$\chi^2$	P
Measured $C_w$	21.5	0.0015**	1.5	0.2176	15.2	0.0185*
Measured $C_m$	27.2	0.0001***	4.7	0.0298*	20.0	0.0028**
Measured $C_{ab}$	17.2	0.0085**	2.3	0.1269	12.0	0.0625
Measured LAI	22.2	0.0011**	6.7	0.0097**	7.1	0.3131
Fieldspec NDVI	21.0	0.0019**	6.3	0.0118*	4.4	0.6287
Fieldspec NDWI	22.5	0.0010***	4.2	0.0410*	8.5	0.2011
Fieldspec PRI	10.9	0.0930	0.6	0.4343	3.9	0.6959
Crop Circle NDVI	12.0	0.0613	4.4	0.0350*	5.5	0.4782
PLSR $C_w$	33.9	0.0000***	5.5	0.0190*	6.5	0.3729
PLSR $C_m$	27.3	0.0001***	7.1	0.0078**	6.3	0.3871
PLSR $C_{ab}$	12.2	0.0575	13.2	0.0003***	2.0	0.9167
PLSR LAI	11.4	0.0779	6.6	0.0103*	11.8	0.0661
PS RMSE $C_w$	3.8	0.6978	1.1	0.2996	6.1	0.4154
PS RMSE $C_m$	24.7	0.0004***	0.8	0.3664	11.1	0.0846
PS RMSE $C_{ab}$	10.9	0.0902	7.3	0.0067**	7.9	0.2487
PS RMSE LAI	10.3	0.1118	2.2	0.1385	7.5	0.2739
PS RMSE N	33.9	0.0000***	3.6	0.0576	2.4	0.8786
PS RMSE $\theta_l$	10.3	0.1145	0.3	0.5744	6.3	0.3869
PS RMSE $s$	8.0	0.2410	3.4	0.0666	1.7	0.9457
PS $\alpha C_w$	11.5	0.0746	0.6	0.4240	5.3	0.5013
PS $\alpha C_m$	5.4	0.4925	6.9	0.0086**	6.8	0.3439
PS $\alpha C_{ab}$	14.7	0.0226*	4.0	0.0460*	11.8	0.0669
PS $\alpha$ LAI	15.1	0.0191*	4.0	0.0451*	6.8	0.3415
PS $\alpha$ N	16.6	0.0111*	0.0	0.9072	12.9	0.0444*
PS $\alpha \theta_l$	22.5	0.0010***	0.3	0.6145	5.0	0.5386
PS $\alpha s$	22.3	0.0011**	7.3	0.0070**	4.6	0.5909

<sup>a</sup>  $\chi^2$ : Chi square statistic,  $\chi^2$ ; hot spot size,  $s$ ; leaf area index, LAI; leaf chlorophyll  $a + b$  content,  $C_{ab}$ ; leaf inclination angle,  $\theta_l$ ; leaf structural coefficient, N; leaf water thickness,  $C_w$ ; normalized difference vegetation index, NDVI; normalized difference water index, NDWI; partial least squares regression, PLSR; physiological (or photochemical) reflectance index, PRI; probability value, P; PROSAIL canopy reflectance model, PS; root mean squared error, RMSE; specific leaf mass,  $C_m$ ; spectral angle,  $\alpha$ .

\*  $p < 0.05$ .

\*\*  $p < 0.01$ .

\*\*\*  $p < 0.001$ .

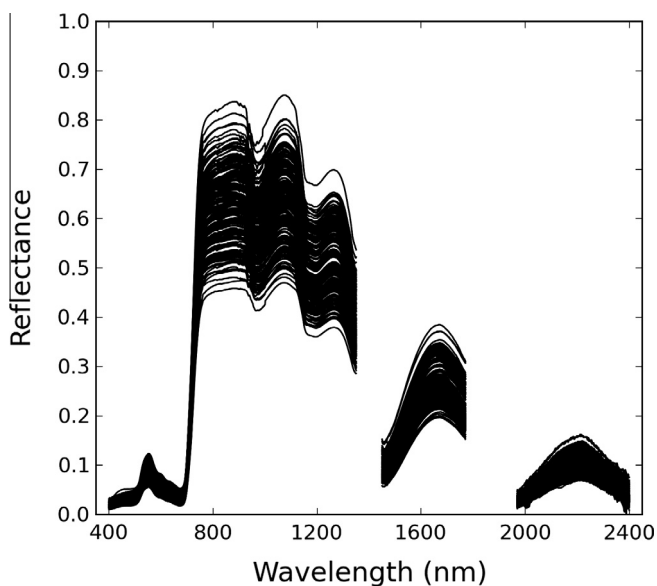


**Fig. 2.** Cotton canopy spectral reflectance measurements for the 2010A, 2010B, 2011, 2012A, and 2012B data sets.

found among cultivars or water levels. Also, unlike NDVI from the spectroradiometer, no differences in NDVI from the Crop Circle sensors were found among cultivars. With a coefficient of determination ( $r^2$ ) of only 0.26 (not shown), the relationship between

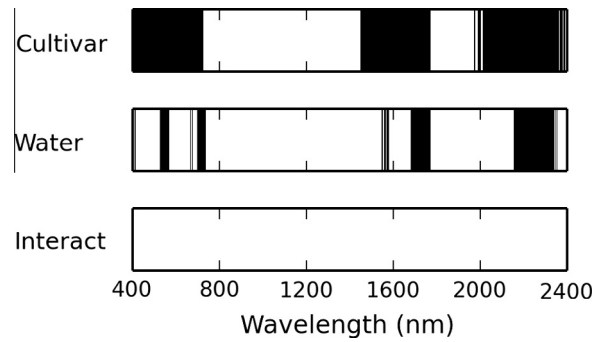


**Fig. 3.** Results of hierarchical linear mixed modeling for canopy spectral reflectance from 400 to 2400 nm in 1 nm wavebands. Dark bands indicate different reflectance values among cultivars or water levels ( $p < 0.05$ ). There were no significant interaction effects.

Fieldspec NDVI and Crop Circle NDVI was weak. This was likely related to different fields-of-view, measurement heights, and light sources among the two sensors. Effects of soil background in the instrument field-of-view was likely more of an issue for the tractor-mounted Crop Circle than for the hand-held spectroradiometer.

Many of the narrow-band NDVI calculations were different among cultivars ( $p < 0.05$ , Fig. 4). When NDVI was computed using a waveband from 400 to 1350 nm and any other waveband, the values often varied among cultivars ( $p < 0.05$ ). An exception was apparent when a red edge band was used with any band greater than 1450 nm. Also, as shown in Table 3, the wavebands used for PRI (i.e., 531 and 570 nm), which is itself a narrow-band NDVI, did not lead to differences. Fewer differences among cultivars were noted when NDVI was calculated using two wavebands greater than 1970 nm. Fewer waveband combinations led to narrow-band NDVI differences among water levels (Fig. 4). Notably, wavebands used for NDWI calculation (i.e., approximately 1240 and 858 nm) led to different narrow-band NDVI among water levels ( $p < 0.05$ ). Narrow-band NDVIs often did not demonstrate significant cultivar by water level interactions, although significant interaction effects were more common when two wavebands in either the near-infrared (i.e., 730–1000 nm) or shortwave infrared (i.e., 1450–1770 nm) were used.

Linear regression models to estimate the measured crop phenotypes from the vegetation indices were unfavorable compared to PLSR models, discussed in the next section. None of the indices could estimate  $C_w$ ,  $C_m$ ,  $C_{ab}$ , and LAI with root mean squared errors better than 9.6%, 16.9%, 14.2%, and 28.8%, respectively. Cross-validated estimates from PLSR were better than the estimates from linear relationships with vegetation indices. For LAI and  $C_{ab}$ , this result differed from that of Hansen and Schjoerring (2003), but they compared narrow-band NDVI with PLSR and did not have spectral reflectance measurements beyond 900 nm. Due to the linear nature of the regression models, another concern is that the statistical results for traits estimated in this way (not shown) were identical to that for the vegetation index itself (Table 3). Thus, using linear regression to estimate traits from vegetation indices did not provide any new information for hierarchical linear mixed modeling.

### 3.3. PLSR modeling

The PLSR models developed from 1703 wavebands of canopy spectral reflectance estimated  $C_w$ ,  $C_m$ ,  $C_{ab}$ , and LAI with RMSECV of 6.8%, 10.9%, 13.1%, and 18.5%, respectively (Fig. 5). Full spectrum data reduced root mean squared errors between measured and modeled phenotypes as compared to vegetation indices using

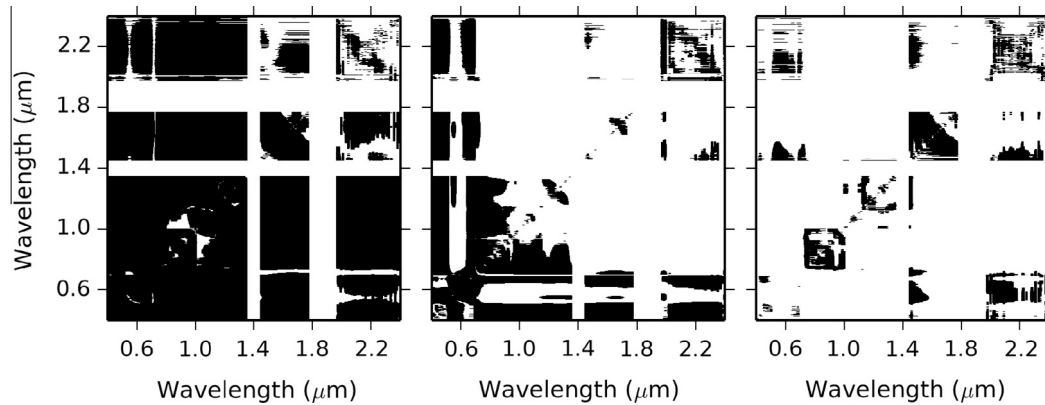


**Fig. 4.** Results of hierarchical linear mixed modeling for narrow-band NDVI calculated using all possible combinations of canopy spectral reflectance in 1 nm wavebands from 400 to 1350 nm, 1450 to 1770 nm, and 1970 to 2400 nm. Dark areas indicate different NDVI values ( $p < 0.05$ ) for the specified wavelengths among cultivars (left), water levels (middle), and their interaction (right).

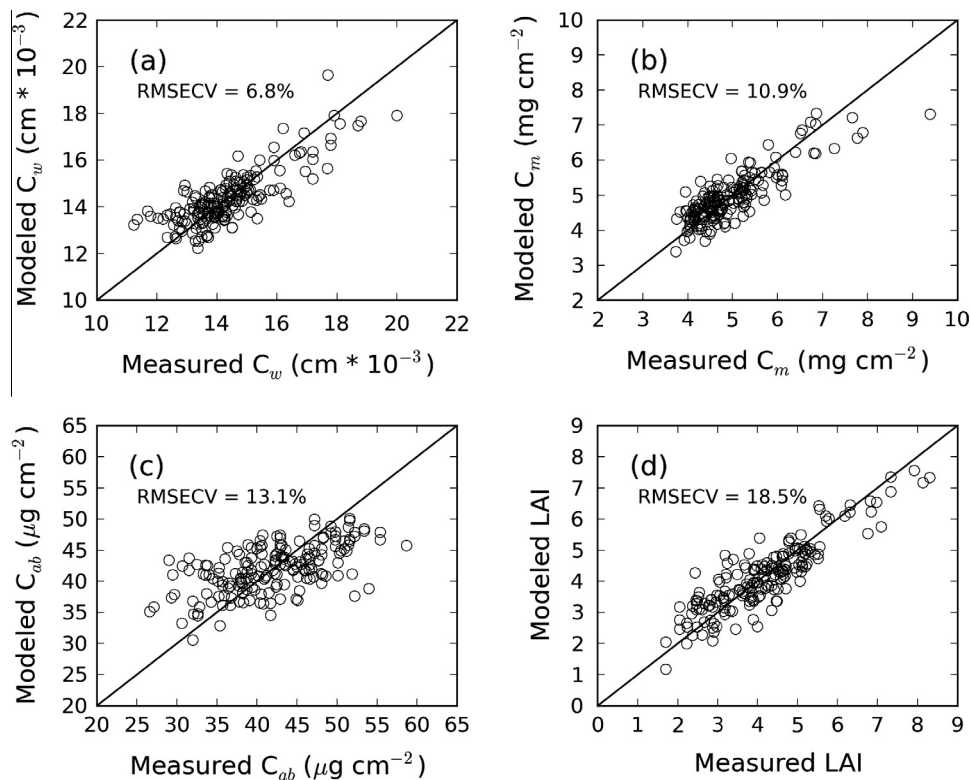


**Fig. 5.** Modeled versus measured (a) leaf water content ( $C_w$ ), (b) specific leaf mass ( $C_m$ ), (c) leaf chlorophyll  $a + b$  content ( $C_{ab}$ ), and (d) leaf area index (LAI). Modeled estimates are from partial least squares regression (PLSR) models developed from measured canopy spectral reflectance data collected for the 2010A, 2010B, 2011, 2012A, and 2012B data sets. The root mean squared errors of cross validation (RMSECV) between measured and modeled values are provided.

reflectance in select wavebands. Additionally, the PLSR results were cross-validated, so the PLSR models have been properly tested with independent data.

Although the PLSR models provided better trait estimates than other techniques, hierarchical linear mixed modeling results for PLSR estimates were somewhat different than that for the field measurements (Table 3). Whereas field-measured  $C_w$ ,  $C_m$ ,  $C_{ab}$ , and LAI were all different among cultivars, the PLSR estimates were different only for  $C_w$  and  $C_m$  ( $p < 0.01$ ). Also, whereas field measurements were different among water levels only for  $C_m$  and LAI, the PLSR estimates for all four traits were different among water levels ( $p < 0.05$ ). Thus, the PLSR technique led to different trait estimates among cultivars and water levels, but the results did not always corroborate results for the field-measured traits.

### 3.4. PROSAIL simulations

Most biophysical models like PROSAIL were not originally designed with high-performance computing in mind. Thus, efforts to use such models on supercomputers demonstrate what is possible with modern computing resources. Using the Fortran-compiled PROSAIL model, which required hard disk access for model input and output, 40 million simulations were completed in 40.4 h for an average of 275 simulations per second. However, when using the PROSAIL model compiled as a Python extension, 3.68 billion simulations were completed in 37.3 h for an average of 27,395 simulations per second. Simulations could be multiplied 100 times by using a model that did not require hard drive access.



Storage requirements were also a concern for the PROSAIL simulation exercises. For trials with the Fortran-based PROSAIL model, the overall job size was small enough to write simulated reflectance data in 1703 wavebands to the hard disk. Using binary files to write reflectance data as 4-digit integers, simulated data for 40 million PROSAIL runs required 136.4 GB of storage. Increasing the job size to 3.68 billion would thus increase storage requirements to several TB, which exceeded allocation limits on Stampede. Therefore, only the RMSE (Eq. (7)) and  $\alpha$  (Eq. (8)) metrics were stored for the larger job, which required only 36 GB. Decisions like these are central to the design of supercomputing jobs for models like PROSAIL.

### 3.5. PROSAIL model inversion

For the PROSAIL model inversion with the objective to minimize RMSE between measured and simulated canopy spectral reflectance in 1703 wavebands (Eq. (7)),  $C_w$ ,  $C_m$ ,  $C_{ab}$ , and LAI were estimated with RMSE of 37.6%, 31.1%, 16.6%, and 29.5%, respectively (Fig. 6). When the objective was to minimize  $\alpha$  between measured and simulated canopy spectral reflectance (Eq. (8)),  $C_w$ ,  $C_m$ ,  $C_{ab}$ , and LAI were estimated with RMSE of 38.1%, 36.1%, 15.9%, and 28.2%, respectively. Clearly, results from both objective functions were inferior to that from PLSR models (Fig. 5). Discrepancies between measured and simulated  $C_w$  suggested problems in how PROSAIL simulated effects of leaf-level water content on canopy-level spectral reflectance (Fig. 6a). Inversions with both objective functions resulted in higher  $C_w$  than measured, and many optimum  $C_w$  estimates were near the imposed upper bound of 0.02 cm (Table 2). This effect did not occur when reflectance in 501 wavebands from 400 nm to 900 nm were used for PROSAIL model inversion. In this case, RMSE between measured and simulated values dropped from

38% to 23% (not shown). Thus, discrepancies in the near-infrared wavebands above 900 nm and the shortwave infrared wavebands (discussed below) likely drove the high error between simulated and measured  $C_w$ . This result highlights the potential for model inversion outcomes to be affected by methodological choices. Estimates of  $C_m$  based on minimum RMSE were often underestimated, while  $C_m$  based on minimum  $\alpha$  were overestimated for all but a few cases (Fig. 6b). With high RMSE and low correlation between measured and simulated values,  $C_w$  and  $C_m$  were the most difficult parameters to estimate using PROSAIL model inversion.

Estimates of  $C_{ab}$  from PROSAIL model inversion were more reasonable (Fig. 6c), although the RMSEs between measured and simulated  $C_{ab}$  were still approximately 3% higher than that for the PLSR model. Estimates of LAI were most problematic for values greater than 6.0 (Fig. 6d). Measurement error is likely partially responsible for this result, because LAI measurements were based on Crop Circle NDVI and canopy height according to Eq. (5). Some cultivars reached over 1.5 m in height, but Eq. (5) was parameterized using data from cotton with height less than 1.1 m. Thus, the higher LAI “measurements” suffered from extrapolation issues. When removing the LAI values above 6.0 from the calculation, the RMSE between measured and simulated LAI was still above 22% which was 4% higher than that for the PLSR model with all data included.

When the objective was to minimize RMSE between measured and simulated canopy spectral reflectance, the resulting deviation between PROSAIL-simulated and measured spectral reflectance was not greater than 0.05 at any wavelength (Fig. 7a). In fact, simulated reflectance could often be optimized to within 0.02 of measured reflectance for most wavelengths. This showed that the inversion approach worked appropriately to find parameter values that achieved the best fit between PROSAIL-simulated and measured canopy spectral reflectance. When measured values for

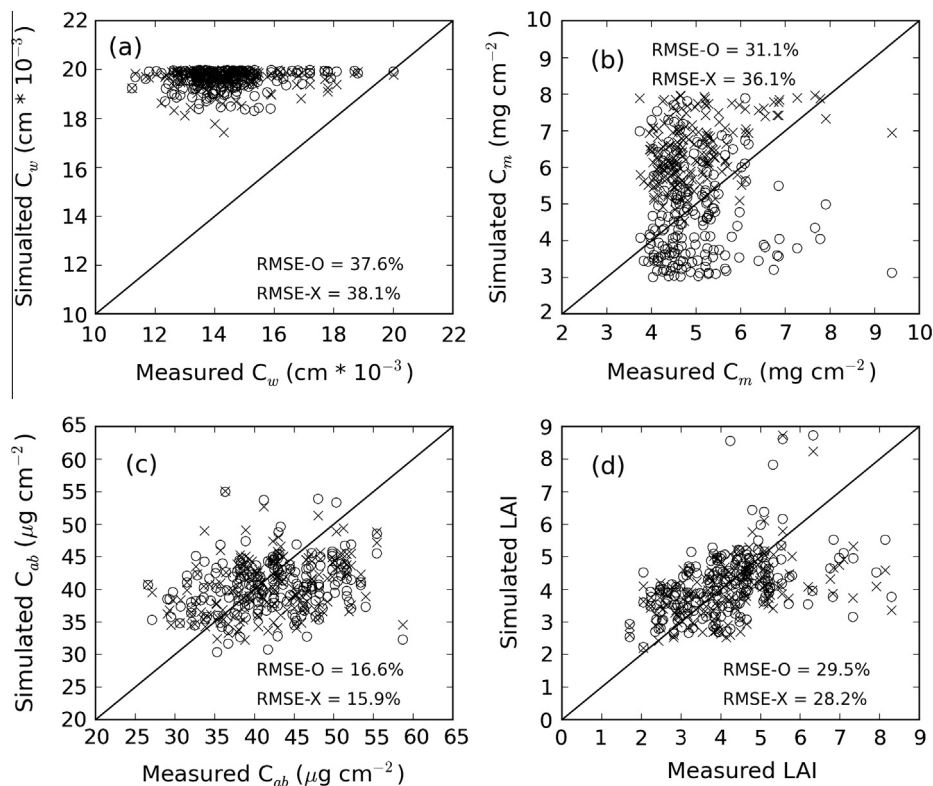


**Fig. 6.** PROSAIL-simulated versus measured (a) leaf water content ( $C_w$ ), (b) specific leaf mass ( $C_m$ ), (c) leaf chlorophyll a + b content ( $C_{ab}$ ), and (d) leaf area index (LAI). Simulated estimates minimized the root mean squared error (O) or the spectral angle (X) between measured and PROSAIL-simulated canopy spectral reflectance for the 2010A, 2010B, 2011, 2012A, and 2012B data sets. Root mean squared errors between simulated and measured values are provided for both objective functions (RMSE-O and RMSE-X).

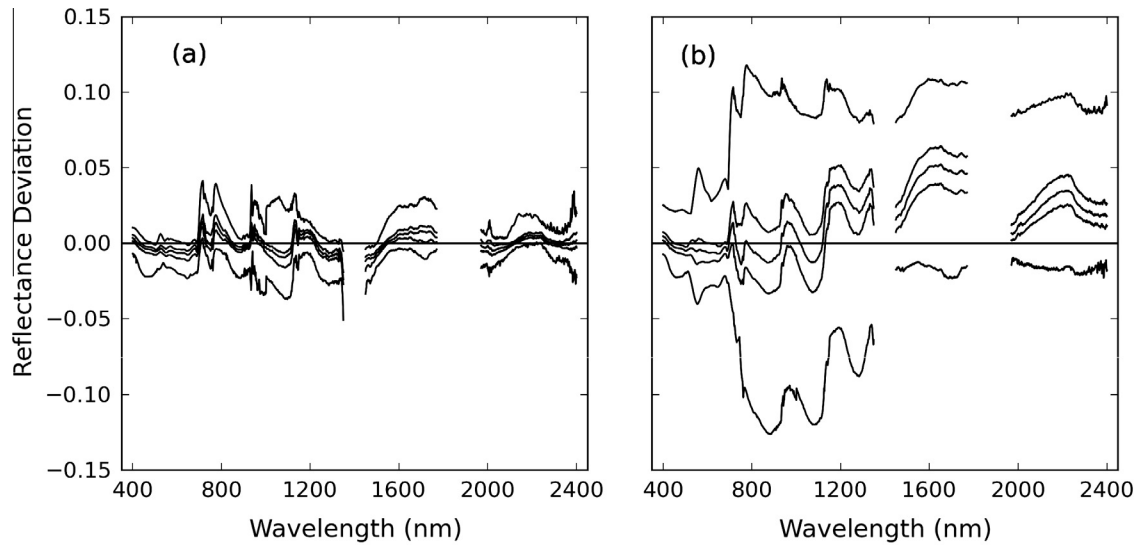


**Fig. 7.** Minimum, lower quartile, median, upper quartile, and maximum deviations between PROSAIL-simulated and measured canopy spectral reflectance for (a) the PROSAIL model inversion that minimized RMSE and (b) subsequently replacing the optimum values for leaf water content ( $C_w$ ), specific leaf mass ( $C_m$ ), leaf chlorophyll  $a + b$  content ( $C_{ab}$ ), and leaf area index (LAI) with measured values.

$C_w$ ,  $C_m$ ,  $C_{ab}$ , and LAI were then substituted for the values obtained through PROSAIL model inversion, the resulting deviations between PROSAIL-simulated and measured canopy spectral reflectance (Fig. 7b) explain why PROSAIL model inversion had problems producing accurate values for these parameters. Foremost, there were greater positive deviations in reflectance from 1100 to 2400 nm. Thus, the model overestimated reflectance in these wavebands when measured parameters were used. Also, there were greater deviations, up to 0.13, in the near-infrared wavebands from 750 to 1350 nm. These results could indicate errors in both measurement and modeling, and improvements could focus in the mentioned waveband intervals.

Plotting the ranked RMSE and  $\alpha$  statistics for the top 1% (200,000) of PROSAIL evaluations provided insights on equifinality effects (Fig. 8). Results showed rapid departure from the minimum function evaluation within the top 0.1% (20,000) of total model evaluations. Deviations from the minimum function evaluation were less variable for evaluations ranked greater than 20,000, indicating greater equifinality effects with increasing evaluation rank. The results suggest that model inversion identified a relatively small fraction of parameter combinations with low RMSE and  $\alpha$  statistics and that equifinality was more problematic for parameter combinations other than these. Parameter estimates for  $C_w$ ,  $C_m$ ,  $C_{ab}$ , and LAI that better agree with measured values might be found within the top 20,000 evaluations. However, equifinality renders the model inversion less useful above 20,000 evaluations. Results also showed that the  $\alpha$  statistic offered better separation from the minimum function evaluation as compared to the RMSE statistic. Thus, equifinality was less problematic for  $\alpha$  than RMSE, but both statistics were able to identify 0.1% of evaluated parameter combinations as top candidates. Remaining issues include (1) understanding equifinality issues among these top candidates and (2) addressing measurement and modeling errors to insure estimated parameters are more accurate (Fig. 6).

Although PROSAIL model inversion estimated phenotypes with less accuracy than other methods, many of the estimates differed among the water level and cultivar treatments imposed during the field studies (Table 3). Results were often inconsistent between the objective functions used for model inversion, which further highlighted the sensitivity of the inversion approach to methodological choices. Generally, more traits were different when the objective was to minimize  $\alpha$  rather than RMSE ( $p < 0.05$ ). Overall

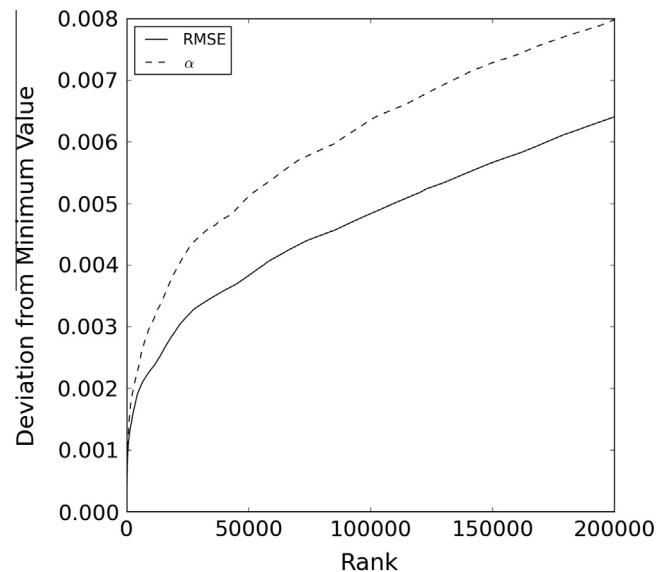


**Fig. 8.** Deviation from the minimum value for ranked objective function evaluations of root mean squared error (RMSE) and spectral angle ( $\alpha$ ) between measured and PROSAIL-simulated canopy spectral reflectance. Results are shown for the median value among model inversion exercises for 184 experimental units (all plots for all five data sets).

results from PROSAIL model inversion were less accurate than that for PLSR models, but differences were nonetheless noted in parameter values estimated by PROSAIL.

#### 4. Discussion

While the differences among the  $C_w$ ,  $C_m$ ,  $C_{ab}$ , and LAI measurements were apparent and biologically meaningful (Table 3), the manual procedures used to quantify these crop phenotypes were labor intensive and time consuming. Though practical here for 4 replications of 5 or even 25 cultivars, obtaining these measurements for 1000 or 10,000 cultivars would amplify labor requirements greatly. Major bottlenecks include labor requirements for collecting and processing leaf samples as well as time required for chemical extraction of  $C_{ab}$  and oven drying to obtain  $C_w$  and

$C_m$ . Thus, proximal or remote sensing metrics that are able to discriminate these crop phenotypes are essential for practical scaling of field-based plant phenomics experiments.

High-throughput approaches are needed for collection of field-based proximal hyperspectral data. Time was the main limiting factor for the manual approaches used in the present study. Six to twelve scans were collected in each of 40 experimental plots in roughly 1.75 h. This provided data for only one-fifth of the cotton cultivars grown in this relatively small study of 25 Pima lines. For larger studies with thousands of lines, high-throughput capability is a necessity. The averaged spectra for each experimental plot were also highly variable in the near-infrared wavebands (Fig. 2), indicating perhaps that more scans per plot were needed to ensure that spectral reflectance of both sunlit and shaded portions of the canopy were adequately characterized. This is important because of the bidirectional reflectance distribution function (BRDF) of the crop canopy, which defines how canopy reflectance properties change with solar and viewer geometry. Because passive spectroradiometers use solar irradiance as the light source, a high-throughput platform for such sensors must also collect data rapidly. This ensures that BRDF effects on canopy spectral reflectance among experimental units are minimal for a given data set. Use of an active field spectroradiometer with its own light source could be another strategy for minimizing BRDF effects, but the authors know of no such instrument for field-based proximal sensing at this time. Finally, a high-throughput platform should enable canopy spectral reflectance measurements from multiple view angles. This would permit better characterization of BRDF effects and would provide more data to constrain PROSAIL model inversion. A high-throughput sensing platform capable of collecting much more than 12 spectral scans from a 8.8 m cotton row at multiple view angles in a few seconds would be ideal for field-based plant phenomics applications. To multiply efforts, sensing units with these characteristics could be distributed along a tractor boom or gantry system or perhaps mounted on a fleet of unmanned aerial systems.

To minimize BRDF impacts on canopy reflectance measurements, passive reflectance sensing is often restricted to times near solar noon. In central Arizona in August, this strategy provides two hours from 11:30 to 13:30 when the solar zenith angle does not change by more than 5°. Another strategy is to maintain constant BRDF effects for spectral data collected over an entire growing season. For cotton in Arizona, spectral measurements around the time of a 45° solar zenith angle permits data collection with similar BRDF characteristics from April to September. In the present study, the goal was to collect spectral measurements concurrently with measurements of  $C_w$ . Because prior studies demonstrated the dynamic diurnal response of  $C_w$  and greater  $C_w$  variability among experimental treatments in the morning (Carmo-Silva et al., 2012), canopy spectral reflectance measurements were primarily collected in the hours before and after solar noon (Table 1). Concurrent spectral measurements with dynamic  $C_w$  was deemed more important than strict adherence to data collection at solar noon, although the average solar zenith during spectral measurements was 42°, similar to the 45° angle required for constant BRDF effects over a cotton season. Crop phenotypes that undergo dynamic diurnal changes could require a departure from traditional passive reflectance sensing techniques that restrict data collection to solar noon. If the optimum time for monitoring a given phenotype occurs while canopy spectral reflectance changes more rapidly due to BRDF effects, efforts must focus on understanding these BRDF effects and on designing sensors and sensing protocols that either characterize or minimize them. For example, multiple view angles assist with BRDF characterization while rapid spectral data collection minimizes illumination changes among experimental units.

The PROSAIL model offers several advantages for field-based plant phenomics, including its ability (1) to simulate BRDF effects on canopy spectral reflectance and (2) to estimate phenotypes from canopy spectral reflectance data alone. This study was limited to spectral reflectance measurements from a nadir view angle, which likely limited efforts to estimate phenotypes using PROSAIL model inversion. Data from multiple view angles should provide more information to constrain PROSAIL, leading to better estimates. There were also many methodological choices that impacted the PROSAIL model inversion results, including the selected wavebands and the objective function. Future efforts should explore these issues in greater detail. For example, with high-performance computing capabilities, a large database of PROSAIL simulations could be generated and permanently stored. Multiple measurement sets of a large mapping population over multiple years and locations could then be inverted using the same database. Also, the data could be used to develop confidence regions within the parameter space, which would assist with parameter identification and equifinality issues.

As compared to PROSAIL model inversion, methods involving linear regression on vegetation indices and PLSR on canopy spectral reflectance were able to better quantify crop phenotypes. At this time, these methods remain the most practical approach for crop phenotyping based on canopy spectral reflectance. A main drawback of the regression approaches is that field measurements of each phenotype are required for model fitting. A practical approach for field phenomics may be to directly measure phenotypes for selected experimental plots and to measure canopy spectral reflectance over all plots using a high-throughput sensing platform. Data from plots with both types of measurements could be used for building regression models, which would subsequently be applied to estimate phenotypes for all experimental units.

## 5. Conclusions

Proximal hyperspectral sensing offers a wealth of information for characterizing reflectance from crop canopies and should be a fundamental component of field-based plant phenomics programs. This study showed that PLSR modeling was the most robust method for estimating  $C_w$ ,  $C_m$ ,  $C_{ab}$ , and LAI from canopy spectral reflectance data. Vegetation indices computed from selected wavebands, including NDVI, NDWI, and PRI, were informative but could not estimate phenotypes as well as PLSR. With improvements to the PROSAIL model and ability to rapidly collect spectral reflectance data from multiple view angles, model inversion for crop phenotyping may become more practical. In the meantime, further investigations are needed to improve PROSAIL model inversion strategies and to address related equifinality issues. High-performance computing offers much potential for these efforts and for overall advancements in the use of biophysical models for agricultural applications.

## Acknowledgments

The authors acknowledge the Texas Advanced Computing Center (TACC) at the University of Texas at Austin for providing high-performance computing resources that contributed to the research results reported in this paper (<http://www.tacc.utexas.edu>). This work is an outgrowth of an iPlant-AgMIP modeling workshop at TACC in 2013. The iPlant Collaborative is acknowledged for sponsoring the workshop and supporting travel for some authors of this paper. Also, Kristen Cox, Joel Gilley, Suzette Maneely, Bradley Roybal, and Sara Wyckoff are acknowledged for technical support. Doug Hunsaker is acknowledged for assistance with irrigation

scheduling. The research was partially supported by National Science Foundation grant DBI-1238187 and Cotton Incorporated.

## References

- Allen, R.G., Pereira, L.S., Raes, D., Smith, M., 1998. Crop Evapotranspiration: Guidelines for Computing Crop Water Requirements. FAO Irrigation and Drainage Paper 56. Food and Agriculture Organization of the United Nations, Rome, Italy.
- Andrade-Sanchez, P., Gore, M.A., Heun, J.T., Thorp, K.R., Carmo-Silva, A.E., French, A.N., Salvucci, M.E., White, J.W., 2014. Development and evaluation of a field-based high-throughput phenotyping platform. *Funct. Plant Biol.* 41 (1), 68–79.
- Araus, J.L., Cairns, J.E., 2014. Field high-throughput phenotyping: the new crop breeding frontier. *Trends Plant Sci.* 19 (1), 52–61.
- Babar, M.A., Van Ginkel, M., Klatt, A., Prasad, B., Reynolds, M.P., 2006. The potential of using spectral reflectance indices to estimate yield in wheat grown under reduced irrigation. *Euphytica* 150 (1–2), 155–172.
- Bajwa, S.G., 2006. Modeling rice plant nitrogen effect on canopy reflectance with partial least square regression (PLSR). *Trans. ASABE* 49 (1), 229–237.
- Bannari, A., Morin, D., Bonn, F., Huete, A.R., 1995. A review of vegetation indices. *Remote Sens. Rev.* 13 (1–2), 95–120.
- Bolger, M.E., Weisshaar, B., Scholz, U., Stein, N., Usadel, B., Mayer, K.F.X., 2014. Plant genome sequencing – applications for crop improvement. *Curr. Opin. Biotechnol.* 26, 31–37.
- Botha, E.J., Leblon, B., Zebbarth, B., Watmough, J., 2007. Non-destructive estimation of potato leaf chlorophyll from canopy hyperspectral reflectance using the inverted PROSAIL model. *Int. J. Appl. Earth Obs. Geoinform.* 9 (4), 360–374.
- Botha, E.J., Leblon, B., Zebbarth, B.J., Watmough, J., 2010. Non-destructive estimation of wheat leaf chlorophyll content from hyperspectral measurements through analytical model inversion. *Int. J. Remote Sens.* 31 (7), 1679–1697.
- Carmo-Silva, A.E., Gore, M.A., Andrade Sanchez, P., French, A.N., Hunsaker, D.J., Salvucci, M.E., 2012. Decreased CO<sub>2</sub> availability and inactivation of Rubisco limit photosynthesis in cotton plants under heat and drought stress in the field. *Environ. Exp. Bot.* 83, 1–11.
- Comar, A., Burger, P., De Solan, B., Baret, F., Daumard, F., Hanocq, J.F., 2012. A semi-automatic system for high throughput phenotyping wheat cultivars in-field conditions: description and first results. *Funct. Plant Biol.* 39 (11), 914–924.
- Combal, B., Baret, F., Weiss, M., Trubuil, A., MacT, D., PragnFre, A., Myneni, R., Knyazikhin, Y., Wang, L., 2003. Retrieval of canopy biophysical variables from bidirectional reflectance using prior information to solve the ill-posed inverse problem. *Remote Sens. Environ.* 84 (1), 1–15.
- Darvishzadeh, R., Matkan, A.A., Dashti Ahangar, A., 2012. Inversion of a radiative transfer model for estimation of rice canopy chlorophyll content using a lookup-table approach. *IEEE J. Sel. Topics Appl. Earth Obs. Remote Sens.* 5 (4), 1222–1230.
- Fu, Y., Yang, G., Wang, J., Song, X., Feng, H., 2014. Winter wheat biomass estimation based on spectral indices, band depth analysis and partial least squares regression using hyperspectral measurements. *Comput. Electron. Agric.* 100, 51–59.
- Furbank, R., Tester, M., 2011. Phenomics – technologies to relieve the phenotyping bottleneck. *Trends Plant Sci.* 16 (12), 635–644.
- Gamon, J.A., Peuelas, J., Field, C.B., 1992. A narrow-waveband spectral index that tracks diurnal changes in photosynthetic efficiency. *Remote Sens. Environ.* 41 (1), 35–44.
- Gao, B.C., 1996. NDWI – a normalized difference water index for remote sensing of vegetation liquid water from space. *Remote Sens. Environ.* 58 (3), 257–266.
- Gutierrez, M., Norton, R., Thorp, K.R., Wang, G., 2012. Association of spectral reflectance indices with plant growth and lint yield in upland cotton. *Crop Sci.* 52 (2), 849–857.
- Hansen, P.M., Schjoerring, J.K., 2003. Reflectance measurement of canopy biomass and nitrogen status in wheat crops using normalized difference vegetation indices and partial least squares regression. *Remote Sens. Environ.* 86 (4), 542–553.
- Houle, D., Govindaraju, D.R., Omholt, S., 2010. Phenomics: the next challenge. *Nat. Rev. Genet.* 11 (12), 855–866.
- Jacquemoud, S., 1993. Inversion of the PROSPECT + SAIL canopy reflectance model from AVIRIS equivalent spectra: theoretical study. *Remote Sens. Environ.* 44 (2–3), 281–292.
- Jacquemoud, S., Baret, F., Andrieu, B., Danson, F.M., Jaggard, K., 1995. Extraction of vegetation biophysical parameters by inversion of the PROSPECT + SAIL models on sugar beet canopy reflectance data. Application to TM and AVIRIS sensors. *Remote Sens. Environ.* 52 (3), 163–172.
- Jacquemoud, S., Verhoef, W., Baret, F., Bacour, C., Zarco Tejada, P.J., Asner, G.P., Frantois, C., Ustin, S.L., 2009. PROSPECT + SAIL models: a review of use for vegetation characterization. *Remote Sens. Environ.* 113 (Suppl. 1), S56–S66.
- Koetz, B., Baret, F., Poilvé, H., Hill, J., 2005. Use of coupled canopy structure dynamic and radiative transfer models to estimate biophysical canopy characteristics. *Remote Sens. Environ.* 95 (1), 115–124.
- Kruse, F.A., Lefkoff, A.B., Boardman, J.W., Heidebrecht, K.B., Shapiro, A.T., Barloon, P. J., Goetz, A.F.H., 1993. The spectral image processing system (SIPS)-interactive visualization and analysis of imaging spectrometer data. *Remote Sens. Environ.* 44 (2–3), 145–163.
- Mevik, B.H., Wehrens, R., 2007. The pls package: principle component and partial least squares regression in R. *J. Stat. Softw.* 18 (2), 1–24.
- Mistele, B., Schmidhalter, U., 2008. Spectral measurements of the total aerial N and biomass dry weight in maize using a quadrilateral-view optic. *Field Crops Res.* 106 (1), 94–103.
- Montes, J.M., Melchinger, A.E., Reif, J.C., 2007. Novel throughput phenotyping platforms in plant genetic studies. *Trends Plant Sci.* 12 (10), 433–436.
- Montes, J.M., Technow, F., Dhillon, B.S., Mauch, F., Melchinger, A.E., 2011. High-throughput non-destructive biomass determination during early plant development in maize under field conditions. *Field Crops Res.* 121 (2), 268–273.
- Porra, R.J., Thompson, W.H., Kriedemann, P.E., 1989. Determination of accurate extinction coefficients and simultaneous equations for assaying chlorophylls a and b extracted with four different solvents: verification of the concentration of chlorophyll standards by atomic absorption spectroscopy. *Biochim. Biophys. Acta* 975 (3), 384–394.
- Reda, I., Andreas, A., 2004. Solar position algorithm for solar radiation applications. *Sol. Energy* 76 (5), 577–589.
- Rundquist, D., Perk, R., Leavitt, B., Keydan, G., Gitelson, A., 2004. Collecting spectral data over cropland vegetation using machine-positioning versus hand-positioning of the sensor. *Comput. Electron. Agric.* 43 (2), 173–178.
- Scotford, I.M., Miller, P.C.H., 2004. Estimating tiller density and leaf area index of winter wheat using spectral reflectance and ultrasonic sensing techniques. *Biosyst. Eng.* 89 (4), 395–408.
- Seelig, H.D., Hoehn, A., Stodieck, L.S., Klaus, D.M., Adams III, W.W., Emery, W.J., 2008. The assessment of leaf water content using leaf reflectance ratios in the visible, near-, and short-wave-infrared. *Int. J. Remote Sens.* 29 (13), 3701–3713.
- Thenkabail, P.S., Smith, R.B., DePauw, E., 2000. Hyperspectral vegetation indices and their relationships with agricultural crop characteristics. *Remote Sens. Environ.* 71 (2), 158–182.
- Thorp, K.R., Dierig, D.A., French, A.N., Hunsaker, D.J., 2011. Analysis of hyperspectral reflectance data for monitoring growth and development of lesquerella. *Ind. Crops Prod.* 33 (2), 524–531.
- Thorp, K.R., Steward, B.L., Kaleita, A.L., Batchelor, W.D., 2008. Using aerial hyperspectral remote sensing imagery to estimate corn plant stand density. *Trans. ASABE* 51 (1), 311–320.
- Thorp, K.R., Tian, L., Yao, H., Tang, L., 2004. Narrow-band and derivative-based vegetation indices for hyperspectral data. *Trans. ASAE* 47 (1), 291–299.
- Thorp, K.R., Wang, G., West, A.L., Moran, M.S., Bronson, K.F., White, J.W., Mon, J., 2012. Estimating crop biophysical properties from remote sensing data by inverting linked radiative transfer and ecophysiological models. *Remote Sens. Environ.* 124, 224–233.
- Wanjura, D.F., Hatfield, J.L., 1987. Sensitivity of spectral vegetative indices to crop biomass. *Trans. ASAE* 30 (3), 810–816.
- White, J.W., Andrade Sanchez, P., Gore, M.A., Bronson, K.F., Coffelt, T.A., Conley, M. M., Feldmann, K.A., French, A.N., Heun, J.T., Hunsaker, D.J., Jenks, M.A., Kimball, B.A., Roth, R.L., Strand, R.J., Thorp, K.R., Wall, G.W., Wang, G., 2012. Field-based phenomics for plant genetics research. *Field Crops Res.* 133, 101–112.
- Yang, Y., Ling, P.P., 2004. Improved model inversion procedure for plant water status assessment under artificial lighting using PROSPECT + SAIL. *Trans. ASAE* 47 (5), 1833–1840.
- Zarco-Tejada, P.J., Rueda, C.A., Ustin, S.L., 2003. Water content estimation in vegetation with MODIS reflectance data and model inversion methods. *Remote Sens. Environ.* 85 (1), 109–124.